Crystalline triphenylamine substituted arenes: solid state packing and luminescence properties

*Ajith R. Mallia,[⊥] Remya Ramakrishnan,[⊥] M. A. Niyas and Mahesh Hariharan**

School of Chemistry, Indian Institute of Science Education and Research Thiruvananthapuram, CET Campus, Sreekaryam, Thiruvananthapuram, Kerala, India 695016

Electronic Supplementary Information

Methods

Quantum Yield and lifetime Measurements

Solution state relative quantum yield measurements were performed using quinine sulphate in 0.05 M H_2SO_4 as the reference (reported quantum yield Φ_f =0.546), exciting at 350 nm for NT, AT, PheT and PyT. Fluorescein in ethanol was used as the reference (reported quantum yield Φ_f =0.79) to measure solution state relative quantum yield of PeT exciting at 425 nm. Anthracene in cyclohexane was used as reference (reported quantum yield Φ_f =0.36) to estimate the solution state relative quantum yield of PhT exciting at 340 nm. The solid state quantum yield of ArT derivatives was measured using an integrating sphere for which the accuracy was verified using tris(8-hydroxyquinolinate)aluminium (Alq_3) as a standard and is determined to be 0.37 ± 0.04 (reported quantum yield Φ_f = 0.40).

Lifetime measurements were carried out in an IBH picosecond time correlated single photon counting (TCSPC) system. The detection system consisted of a micro channel plate photomultiplier (5000U-09B, Hamamastu) coupled to a monochromator (500M) and TCSPC electronics (Data station Hub including Hub-NL, NanoLED controller and pre-installed luminescence measurement and analysis studio (FMAS) software. The fluorescence decay profiles were de-convoluted using IBH data station software version 2.1, and fitted with exponential decay, minimizing the χ^2values.Average fluorescence lifetime values were estimated[1] using equation 1.

$$\tau_f = \frac{\alpha_1\tau_1^2 + \alpha_2\tau_2^2 + \alpha_3\tau_3^2 + \ldots}{\alpha_1\tau_1 + \alpha_2\tau_2 + \alpha_3\tau_3 + \ldots} \quad (1)$$

where α_1, α_2, and α_3 corresponds to the amplitudes corresponding to the fluorescence lifetimes τ_1,τ_2, and τ_3 respectively. The average fluorescence lifetime (τ_f) values was used to determine the radiative (k_r) and non-radiative rate constant (k_{nr})[1] as follows,

$$\Phi_f = \frac{k_r}{k_r + k_{nr}} \quad (2)$$

$$k_r = \frac{\Phi_f}{\tau_f} \quad (3)$$

$$k_{nr} = \frac{1-\Phi_f}{\tau_f} \quad (4)$$

Φ_f, denotes solid state fluorescence quantum yield. Variations in Φ_f could be attributed to the changes in k_r or k_{nr}. An enhancement in Φ_f could be attributed to the decrease in the non-radiative (k_{nr}) rate constant.

X-ray crystallography: High-quality specimens of appropriate dimensions were selected for the X-ray diffraction experiments. Crystallographic data collected are presented in the supplementary information. Single crystals were mounted using oil (Infineum V8512) on a glass fibre. All measurements were made on a CCD area detector with graphite monochromated Mo Kα radiation (λ= 0.71073 Å at 298 K). The data was obtained using Bruker APEXII detector and processed using APEX2 from Bruker. All structures were solved by direct methods and expanded using Fourier techniques. The non-hydrogen atoms were refined anisotropically. Hydrogen atoms were included in idealized positions, but not refined. Their positions were constrained relative to their parent atom using the appropriate HFIX command in SHELXL-97.The full validation of CIFs and structure factors of ArT derivatives were performed using CheckCIF and found to be free from major alert level. 3D structure visualization and the exploration of the crystal packing of ArT derivatives were carried out using Mercury 3.8.

Determination of degree of charge separation from Lippert-Mataga plot[2]: The origin of solvent polarity dependent Stokes shifts could be explained using Lippert-Mataga (L-M) plots and Onsager's reaction field model, approximating that a dipole is placed at the center of a vacuum cavity in a homogeneous dielectric medium. The interaction between the solvent and fluorophores affect the energy difference between the ground and excited states and hence the dipoles associated with them. The difference in excited (μ_e) and ground state (μ_g) dipole moments could be expressed as a function of refractive index (n) and dielectric constant (∈) of the medium under consideration and is described as L-M equation as follows,

$$\overline{\vartheta_A} - \overline{\vartheta_F} = \frac{2}{hc}\left(\frac{\epsilon-1}{2\epsilon+1} - \frac{n^2-1}{2n^2+1}\right)\frac{(\mu_e-\mu_g)^2}{a^3} + \text{Constant} \quad (5)$$

wherein, $\overline{\vartheta_A} - \overline{\vartheta_F}$ is the Stokes shift between absorption and emission intensity in respective solvents expressed in wavenumbers (cm^{-1}), '*h*' the Planck's constant in ergs (6.626×10^{-27} ergs), '*c*' the speed of light in cm/s (3×10^{10} cm/s) and '*a*' the Onsager cavity radius in which the fluorophores resides.

A plot of $\Delta\upsilon$, $(\overline{\vartheta_A} - \overline{\vartheta_F})$ against solvent polarisability parameter ($\Delta f = \left(\frac{\epsilon-1}{2\epsilon+1} - \frac{n^2-1}{2n^2+1}\right)$) yields slope equal to $\frac{2(\mu_e-\mu_g)^2}{hca^3}$, from which difference in excited and ground state dipole moment (μ_e- μ_g) could be evaluated as, μ_e- μ_g= $\sqrt{slope \times \frac{hca^3}{2}}$. (Onsager cavity radius is estimated to be 3.74 Å (PhT), 4.03 Å (NT), 4.17 Å (AT), 4.18 Å (PheT), 4.22 Å (PyT) and 4.52 Å (PeT) respectively, from theoretical calculations using B3LYP/6-311+G** level[3] of theory).

The degree of charge separation is estimated as follows, one Debye (1 D) unit is 1.0×10^{-18} esu cm. 4.8 D is the dipole moment that results from a charge separation of one unit charge (4.8×10^{-10} esu) by 1 Å (10^{-8} cm).Conversion of μ_e expressed in Debye into esu Å units is achieved dividing by a factor of 4.8 $esu^{-1}Å^{-1}$ which can provide the experimental charge separation in the molecule. Degree

of charge separation (theoretical) in the molecule is obtained from centers of spin density distributions[4].

Analysis of Chromaticity Index[5]: Coordinates (x, y, z) for chromaticity were acquired by calculating the fractional component of the tristimulus values: x = X/(X+Y+Z), y = Y/(X+Y+Z), z = Z/(X+Y+Z). X, Y, Z are the CIE 1931 tristimulus values. By convention, chromicity coordinates (x, y) denote the two dimensional plot CIE 1931 colour space chromaticity diagram.

Cyclic Voltammetry (CV): Electrochemical measurements were performed on a BASi (Bioanalytical Systems, Inc.) C-3 cell stand controlled by Epsilon electrochemical workstation. A three electrode system is then constructed constituting a glassy carbon as the working electrode, a platinum-wire as the counter electrode, and an Ag/Ag+ (3 M NaCl) as the reference electrode. The electrochemical measurements were conducted under nitrogen atmosphere (5 psi, 10 minutes) in a deoxygenated anhydrous chloroform of tetra-n-butylammonium hexafluorophosphate (supporting electrolyte, 0.1 M) with a scan rate of 50–100 mVs^{-1}. Calibration of the instrument was performed using the ferrocene/ferrocenium (Fc/Fc+) redox couple as an external standard and measured under same condition before and after the measurement of samples. The energy level of Fc/Fc+ was assumed to be –4.8 eV with respect to vacuum[6]. The half-wave potential of Fc/Fc+ was estimated to be 0.5 eV with reference to the Ag/Ag+ electrode.

Computational methods

Single point energy calculations for the ArT monomers were performed at B3LYP/6-311+G** level of theory using the crystal structure data with Gaussian 09 suite[3]. Energy gap is determined as the difference between energies of LUMO and HOMO. Energy level diagram is plotted using the energies obtained from FMO analyses.

Quantum Theory of Atoms in Molecules (QTAIM)[7] **:** The wave function for crystalline ArTs were obtained employing the geometries taken from the crystal structure using Gaussian set of codes at B3LYP/6-311+G** level.[3] Quantum theory of atoms in molecules (QTAIM) analysis helps to understand the description of interatomic interaction in the single crystal X-ray structure. A bond is defined along the bond line between two nuclei, called a bond path, along which electron density is concentrated. The bond critical point (BCP) is a point along the bond path at the interatomic surface, where the shared electron density reaches a minimum. The physical characteristics of the BCPs [the electron density at BCP, $\rho(r)$, and its Laplacian, $\nabla^2\rho(r)$ reveal the approximate measure of the amount of electron density built up in the bonding region and as such could be taken as characteristic of the bond. When $\nabla^2\rho(r) < 0$ and is large in magnitude, $\rho(r)$ is also large which means that there is a concentration of electronic charge in the internuclear region. This is also an indication of a sharing of electronic charge between both nuclei that defines the covalent (polar) bond. When $\nabla^2\rho(r) > 0$ there is a depletion of electronic charge in the internuclear region and it indicates a closed shell interaction. Using the AIM 2000 software package, the electron density was integrated over atomic basins according to the quantum theory of atoms in molecules using PROAIM, and thus the BCP data and the molecular graphs were obtained.

Interacting quantum atoms (IQA)[8] approach was done using AIMALL software to understand the nature of intermolecular interactions. Hamiltonian is partitioned into physical atomic and

interatomic contributions. The energy decomposition computed using partitioned Hamiltonian is consistent with the topological method of quantum theory of atoms in molecules. The interatomic energy contribution values determine the nature of intermolecular or intramolecular interactions.

Electrostatic Surface Potential[9]**:** Electrostatic surface potential map illustrate the charge distributions of molecules three dimensionally. These maps allow us to visualize variably charged regions of a molecule. Knowledge of the charge distributions can be used to determine how molecules interact with one another. Gaussian supports the cube keyword to generate the cubes separately from the formatted checkpoint file using the cubegen utility program. This allows for the generation of electrostatic surface potential mapping of the molecule.

Hirshfeld Analysis[10]**:** Important intermolecular interactions within the crystal structure of ArTs were identified through Hirshfeld surface analysis using Crystal Explorer 3.0. The Hirshfeld surface is defined as a set of points in 3D space where the ratio of promolecule and procrystal electron densities is equal to 0.5. The exploration of intermolecular contacts is provided by mapping normalized contact distances (d_{norm}), which is a function of a closest distance from the point to the nuclei interior (d_i) and exterior (d_e) to the surface as well as on the van der Waals radii (r^{vdw}). 2D fingerprint which were generated by deriving from the Hirshfeld surface by plotting the fraction of points on the surface as the function of d_i and d_e which provide a visual summary of intermolecular contacts within the crystal.

Table S1. Calculated topological properties of the electron density for the intermolecular interaction in ArT derivatives.

Entry	Interactions	[a]d (Å)	[b]ρ(r)(a.u)	[c]∇²ρ(r)(a.u)	[d]ΔE (kJ/mol)
PhTa	C18 - H74	2.869258	0.006167	0.018316	3.784658
	H10 - C84	3.037410	0.004071	0.011319	2.401020
	H8 - H76	2.593224	0.003250	0.010807	2.201482
	H8 - C78	3.245197	0.003061	0.008484	1.895611
	C25 - H85	3.661722	0.001513	0.004689	0.838847
PhTb	H3 - H65	2.275948	0.006164	0.021224	4.286129
	H5 - C51	3.057903	0.003539	0.010728	2.129281
	C38 - H63	3.157225	0.003588	0.010501	2.381329
	H15 - C86	3.067743	0.003339	0.010160	2.093836
	H13 - C53	3.265945	0.003282	0.010081	1.763023
	H15 - N88	3.251315	0.002666	0.009460	2.043952
	H15 - H76	2.851717	0.002228	0.008200	1.382326
NTa	H10 - C53	2.796656	0.006585	0.019875	4.186360
	C9 - H77	3.096091	0.003290	0.009102	1.929743
NTb	C19 - H80	2.801446	0.005829	0.017466	3.550989
	C9 - H75	2.979506	0.005034	0.016243	3.327821
	H4 - C81	3.027458	0.004711	0.013909	2.789594
	H20 - C90	3.085807	0.003749	0.010015	2.242177
	C16 - H91	3.316699	0.002773	0.007919	1.508350
	H38 - H82	3.134481	0.000789	0.003223	0.439771
AT	C11 - H80	2.762195	0.006568	0.019056	3.972382

	C32 - H82	3.076903	0.003594	0.010584	2.273683
PheTa	H28 - C104	2.668934	0.006929	0.020771	4.167981
	C41 - H105	3.113388	0.003586	0.010549	2.444341
	C12 - H89	3.581864	0.001448	0.004489	0.834909
	C8 - H87	3.948631	0.000773	0.002712	0.393825
	H26 - H87	3.326696	0.000544	0.002342	0.270427
	C16 - C78	6.066116	0.000045	0.000145	0.007877
PheTb	H17 - C63	5.333789	0.005763	0.016758	3.674387
	H15 - C61	5.560591	0.004686	0.014297	3.063959
	H19 - C66	5.698480	0.004471	0.012319	2.639940
	H13 - C78	5.702916	0.004262	0.011691	2.638628
	C16 - H82	5.883152	0.003244	0.008800	1.886422
PheTc	H3 - C91	2.797737	0.005762	0.015795	3.369829
	H23 - N112	2.822536	0.005595	0.015440	3.972382
	H23 - H103	2.490894	0.004390	0.015374	3.000947
	H55 - H94	2.540566	0.003441	0.011933	2.391831
	C32 - C93	3.591239	0.003932	0.010805	2.082022
	C54 - H96	3.142948	0.003713	0.010482	2.168663
PyT	H28 - C76	2.837892	0.005676	0.017563	3.662573
	C7 - H91	2.863333	0.004916	0.013894	2.973379
	H30 - C70	2.918995	0.004890	0.013817	3.065271
	C4 - H93	2.924587	0.004811	0.013394	2.910367
	H10 - C99	3.063383	0.004276	0.012203	2.580867
	C12 - C101	3.594224	0.003811	0.012148	2.171289
	H3 - C77	3.079572	0.004112	0.011311	2.294687
	C50 - H68	3.139021	0.003548	0.011203	2.022948
	C52 - H71	3.484526	0.001977	0.006043	1.214294
PeTa	H6 - H8	2.017345	0.012581	0.059869	11.415674
	H70 - H72	2.017432	0.012549	0.059477	11.302778
	H76 - C97	2.547640	0.010816	0.044692	8.591949
	H12 - C33	2.547683	0.010828	0.044689	8.607702
	C25 - H105	2.859843	0.005266	0.015480	3.356702
	C1 - H103	2.864382	0.005470	0.015177	3.277937
	C45 - H66	3.107193	0.004237	0.014141	2.482410
	H22 - H125	2.697149	0.003727	0.012385	2.226424
	H36 - C83	2.968994	0.004431	0.012150	2.618936
	H34 - C81	2.998776	0.004157	0.011698	2.509978
	C9 - H80	3.105926	0.004118	0.011187	2.385267
	C7 - H78	3.091322	0.003916	0.010919	2.322255
	C47 - H86	3.248210	0.003019	0.008718	1.833912
	H2 - C124	3.491959	0.002113	0.006635	1.253676
PeTb	H70 - H72	2.017345	0.012545	0.060247	11.456369
	H6 - H8	2.017345	0.012541	0.059519	11.300152
	H12 - C33	2.547683	0.010835	0.044745	8.628706
	H76 - C97	2.547640	0.010827	0.044697	8.620829
	C33 - H74	2.678831	0.006836	0.021671	4.351766

C19 - H68	3.050146	0.004580	0.013900	2.776466
H46 - H127	2.483759	0.003835	0.012900	2.666195
C29 - H70	3.095787	0.003985	0.012163	2.443028
C15 - H72	3.138475	0.003873	0.011899	2.473221
H46 - C99	3.142016	0.003525	0.010614	2.227737
H44 - C99	3.325228	0.002354	0.008263	1.429585
C45 - H116	3.513555	0.001654	0.005200	0.870353

[a]d=distance, [b]$\rho(r)$=electron density at BCP, [c]$\nabla^2\rho(r)$=Laplacian of electron density at BCP, [d]dE=dissociation energy. a, b and c indicate different dimers of same molecule.

Table S2. Various intermolecular interactions estimated for ArT derivatives from Hirshfeld surface analysis.

Entry	C•••C	C•••H	C•••N	N•••H	H•••H	ρ[(%C•••H)/(%C•••C)]
PhT	0.5 %	36.3 %	0	0.8 %	62.4 %	72.6
NT	1.0 %	36.2 %	0.1 %	0.6 %	62.0 %	36.2
AT	0.4 %	40.5 %	0	0.3 %	58.9 %	101.2
PheT	1.3 %	40.3 %	0.2 %	0.7 %	57.6 %	31.0
PyT	3.2 %	39.5 %	0	0.3 %	57.1 %	12.3
PeT	4.0 %	41.5 %	0	0.6 %	53.6 %	10.4

Table S3. Geometry optimized (B3LYP/6-311+G** level of theory) calculations and redox properties of ArT derivatives using Gaussian 09.

Compounds	Energy (ev)				Eg (ev)
	HOMO-1	HOMO	LUMO	LUMO+1	
PhT	-6.5446	-5.1995	-1.1505	-0.8607	4.0490
NT	-6.0243	-5.2205	-1.3630	-0.8493	3.8575
AT	-5.5435	-5.1193	-1.7638	-0.8634	3.3555
PheT	-6.0344	-5.3549	-1.2838	-1.2569	4.0711
PyT	-5.6509	-5.1454	-1.7489	-0.9260	3.3965
PeT	-5.4581	-4.9821	-2.2109	-0.9181	2.7712

Table S4. Fluorescence Quantum yield (ϕ_f) of aromatic hydrocarbons.

Ar	ϕ_f	
	Solution State	Solid State
Benzene	0.06[a]	-
Naphthalene	0.23[a]	-
Anthracene	0.28[11]	0.64[11]
Phenanthrene	0.13[a]	-
Pyrene	0.32[12]	0.68[11]
Perylene	0.94[a]	0.31[11]

a-Brouwer, A.M., *Pure Appl. Chem*. **2011**, *83*, 2213.

Table S5. Quantum yield (ϕ_f) of ArT derivatives in different solvents.

Solvent	PhT	NT	AT	PheT	PyT	PeT
Hexane	0.41	0.40	0.24	0.36	0.60	0.40
Toluene	0.69	0.51	0.32	0.49	0.78	0.57
DCM	0.51	0.41	0.37	0.64	0.61	0.41
Tetrahydrofuran	0.41	0.43	0.30	0.42	0.59	0.46
Acetonitrile	0.49	0.49	0.29	0.52	0.60	0.41

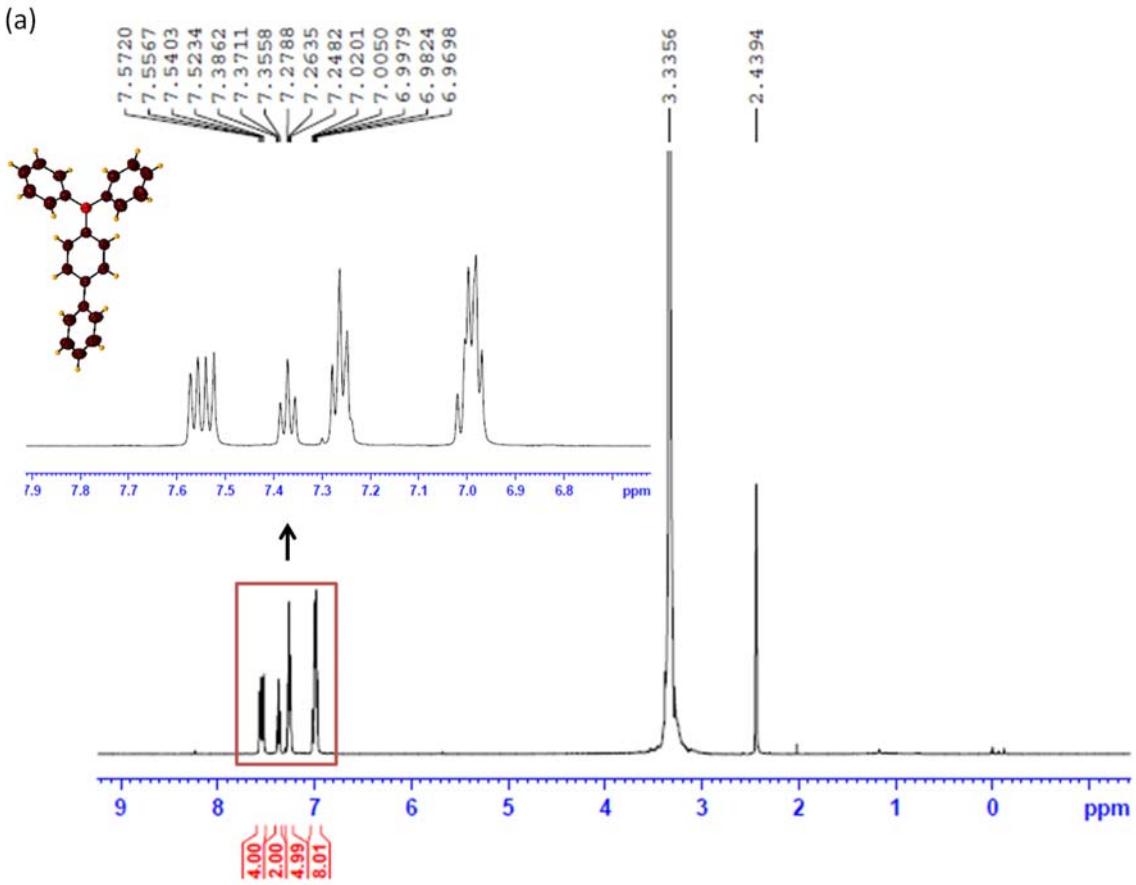
(a)
7.5720
7.5567
7.5403
7.5234
7.3862
7.3711
7.3558
7.2788
7.2635
7.2482
7.0201
7.0050
6.9979
6.9824
6.9698
3.3356
2.4394
7.9 7.8 7.7 7.6 7.5 7.4 7.3 7.2 7.1 7.0 6.9 6.8 ppm
9 8 7 6 5 4 3 2 1 0 ppm
4.00
2.00
4.99
8.01

(b)

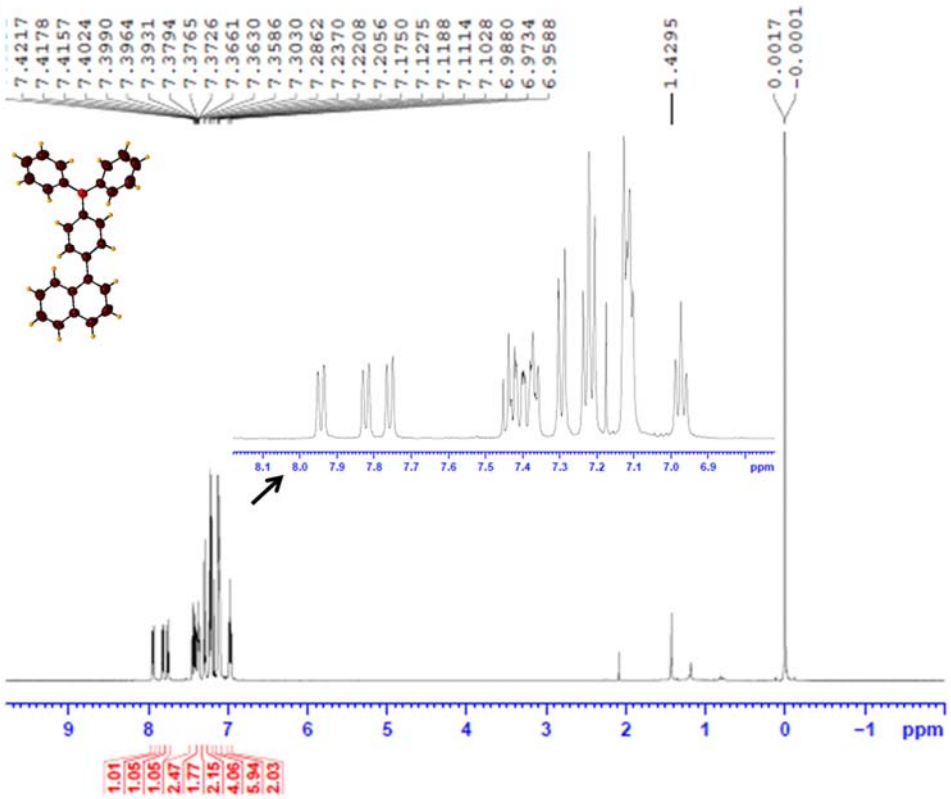
7.4217
7.4178
7.4157
7.4024
7.3990
7.3964
7.3931
7.3794
7.3765
7.3726
7.3661
7.3630
7.3586
7.3030
7.2862
7.2370
7.2208
7.2056
7.1750
7.1275
7.1188
7.1114
7.1028
6.9880
6.9734
6.9588
1.4295
0.0017
-0.0001
ppm
1.01
1.05
1.06
2.47
1.77
2.15
4.06
5.94
2.03

(c)

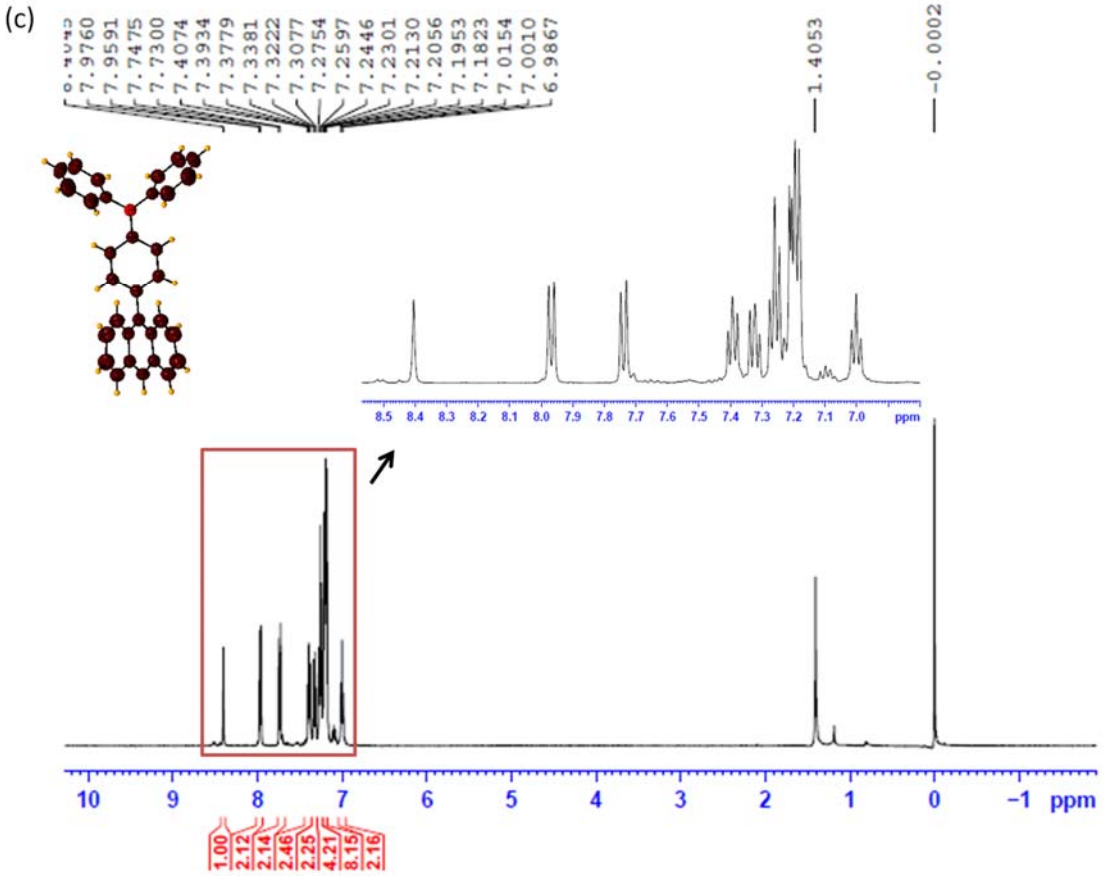
7.9760
7.9591
7.7475
7.7300
7.4074
7.3934
7.3779
7.3381
7.3222
7.3077
7.2754
7.2597
7.2446
7.2301
7.2130
7.2056
7.1953
7.1823
7.0154
7.0010
6.9867
1.4053
-0.0002
ppm
1.00
2.12
2.14
2.46
2.25
4.21
8.15
2.16

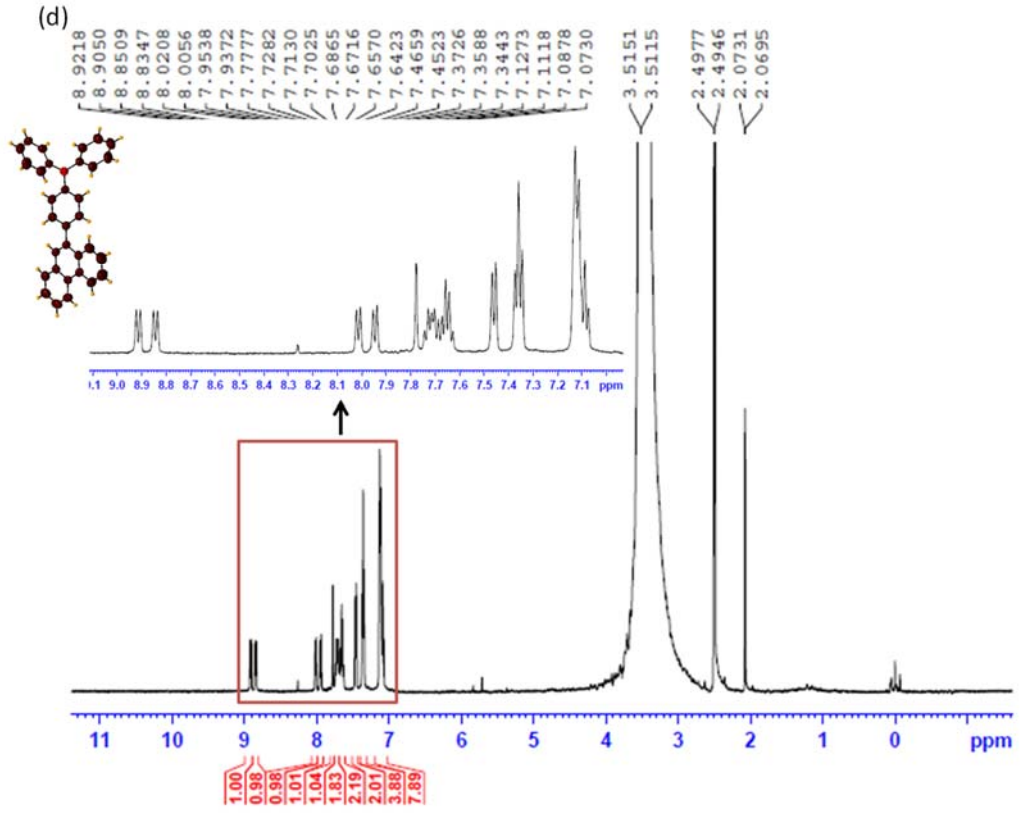
(d)
8.9218
8.9050
8.8509
8.8347
8.0208
8.0056
7.9538
7.9372
7.7777
7.7282
7.7130
7.7025
7.6865
7.6716
7.6570
7.6423
7.4659
7.4523
7.3726
7.3588
7.3443
7.1273
7.1118
7.0878
7.0730
3.5151
3.5115
2.4977
2.4946
2.0731
2.0695
11 10 9 8 7 6 5 4 3 2 1 0 ppm
1.00 0.98 0.98 1.01 1.04 1.83 2.19 2.01 3.88 7.89

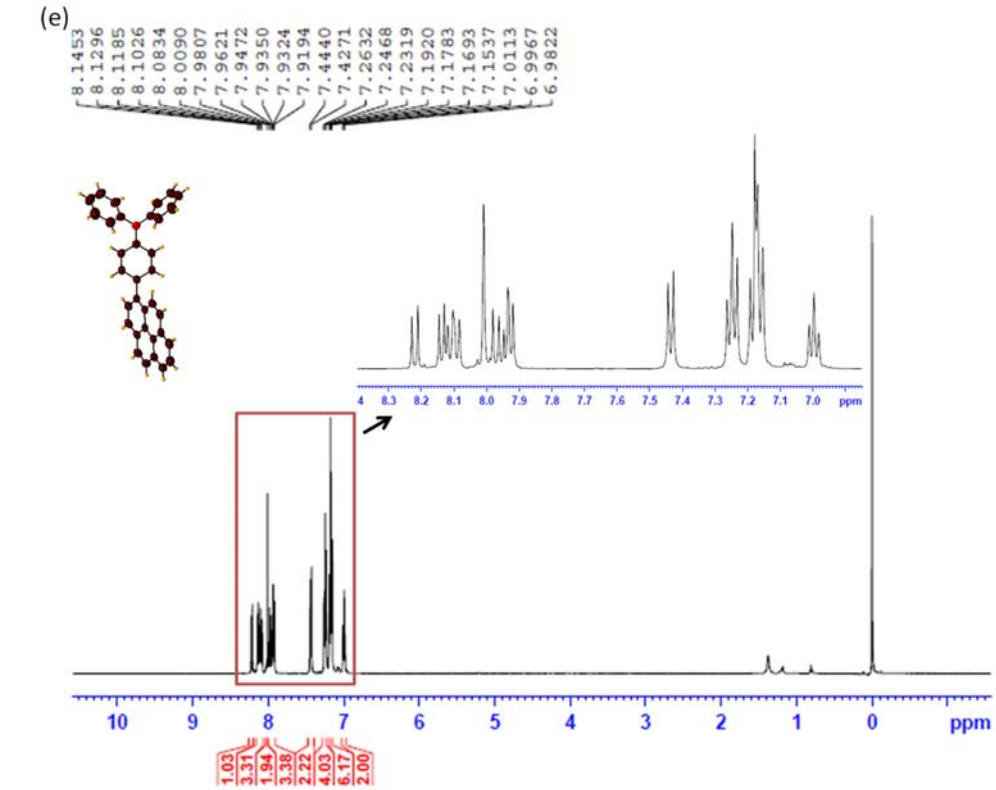
(e)
8.1453
8.1296
8.1185
8.1026
8.0834
8.0090
7.9807
7.9621
7.9472
7.9350
7.9324
7.9194
7.4440
7.4271
7.2632
7.2468
7.2319
7.1920
7.1783
7.1693
7.1537
7.0113
6.9967
6.9822
10 9 8 7 6 5 4 3 2 1 0 ppm
1.03 3.31 1.94 3.38 2.22 4.03 6.17 2.00

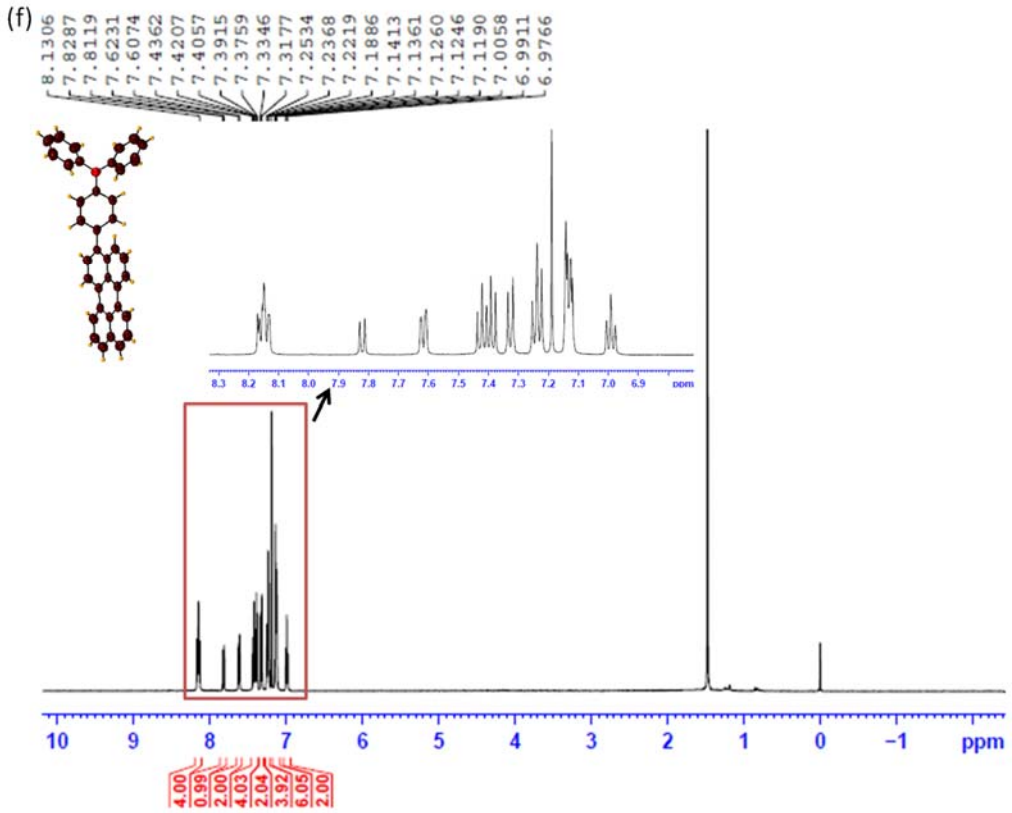

Fig. S1 ^{1}H-NMR spectra of (a) PhT, (b) NT, (c) AT, (d) PheT, (e) PyT and (f) PeT.

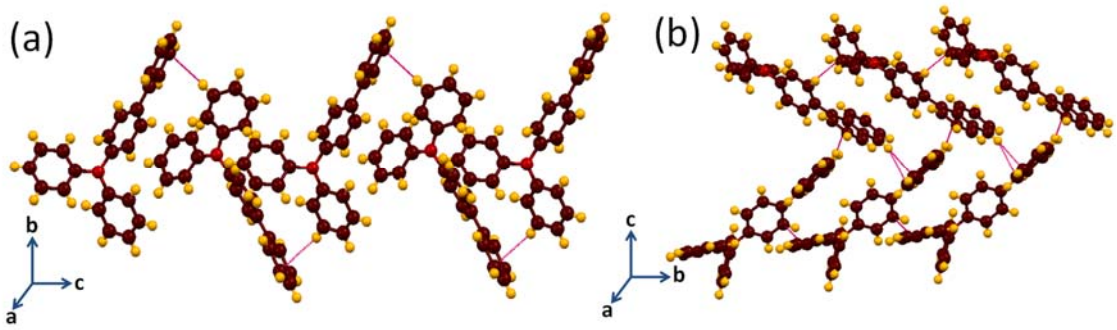

Fig. S2 (a) C-H•••C directed zig-zag arrangement in PhT and (b) duplex structure in NT.

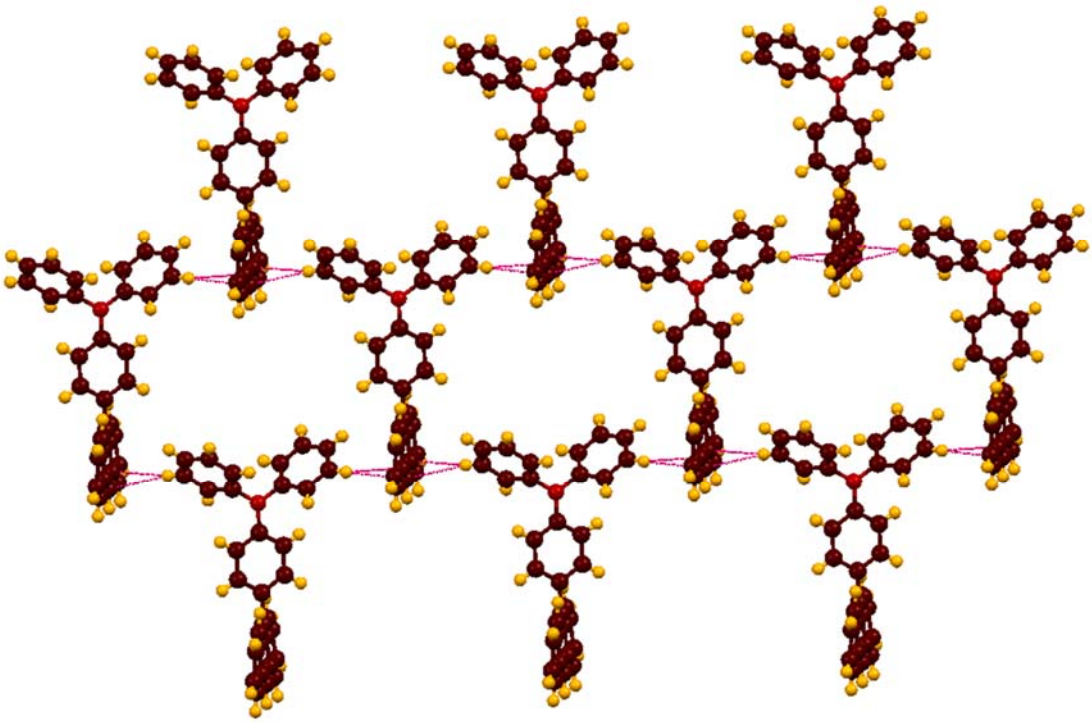

Fig. S3 C-H•••C directed 2D-network in AT.

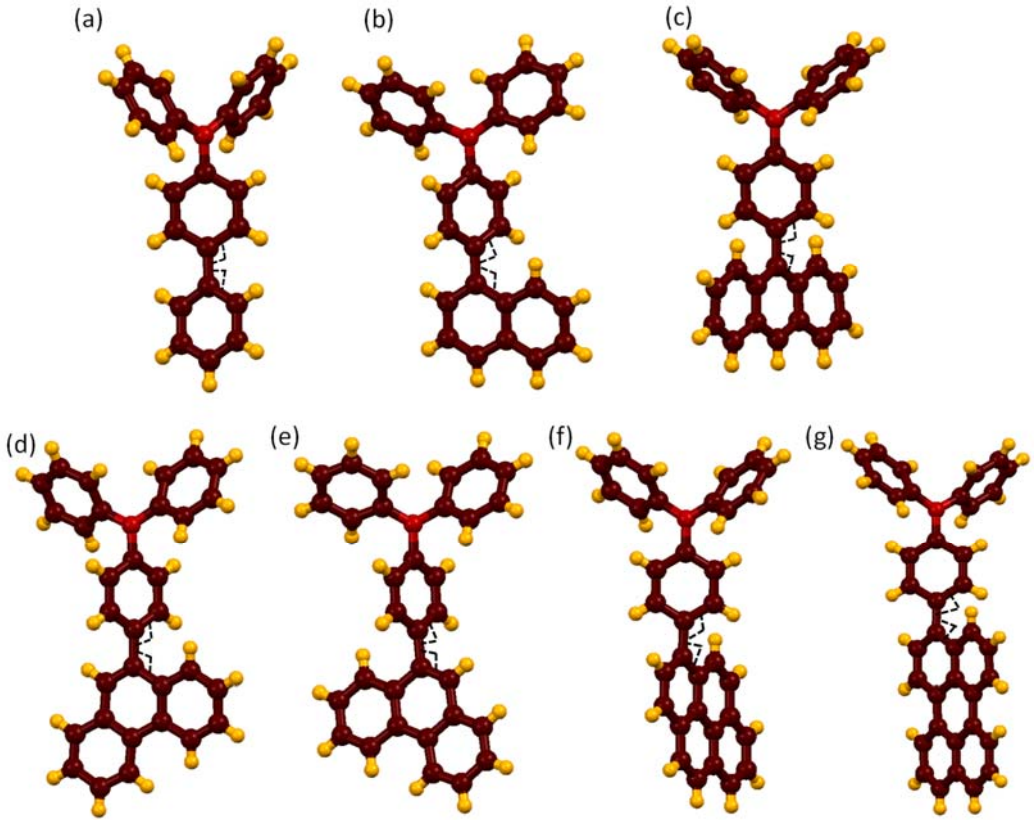

Fig. S4 Torsion angles between Ar and T units in (a) PhT, (b) NT, (c) AT, (d-e) PheT, (f) PyT and (g) PeT (torsion angle is measured across the labelled bonds).

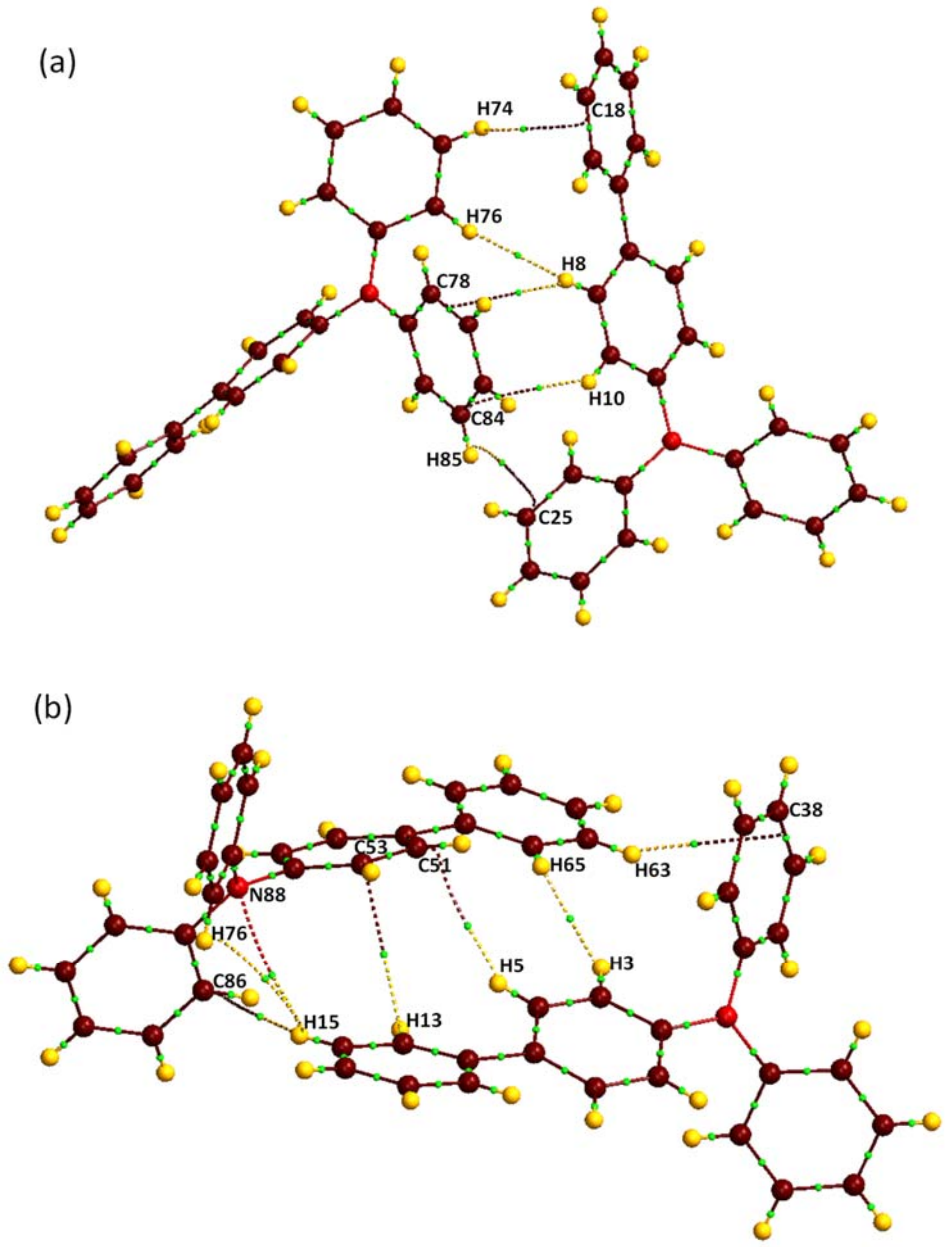
(a)
H74
C18
H76
H8
C78
H10
C84
H85
C25
(b)
C38
C53
C51
H65
H63
N88
H76
H5
H3
C86
H15
H13

(c)

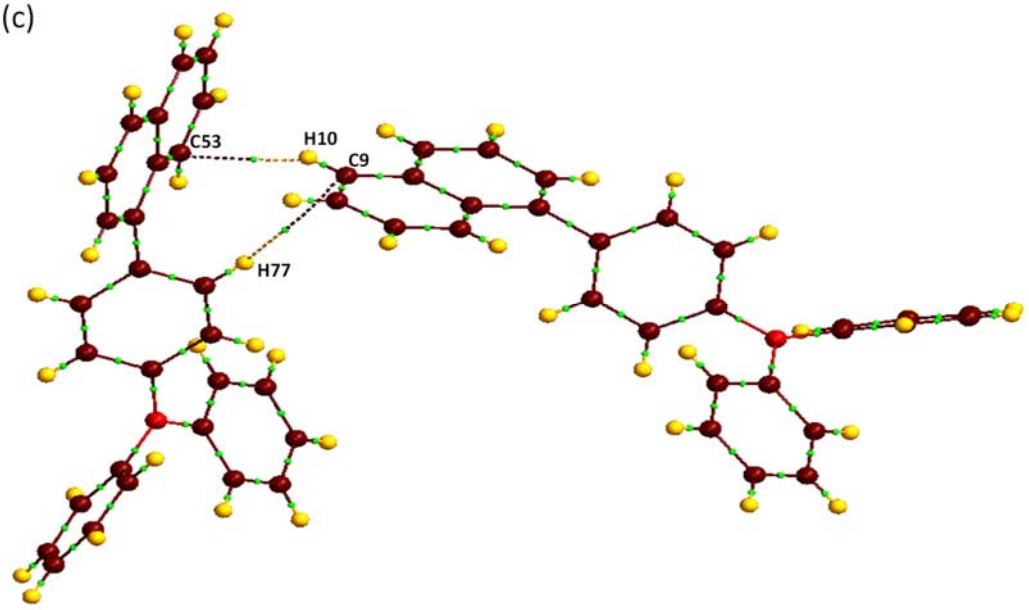

(d)

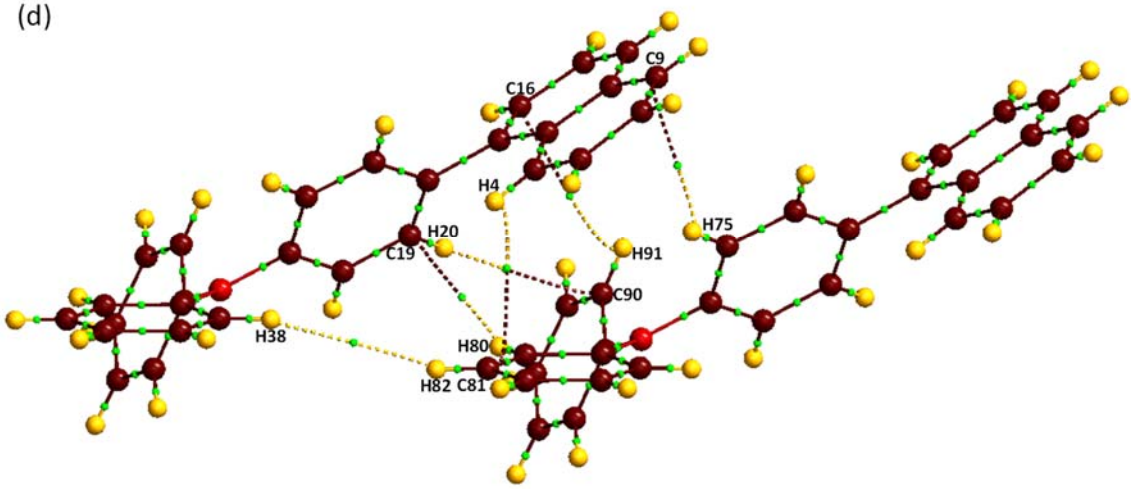

(e)

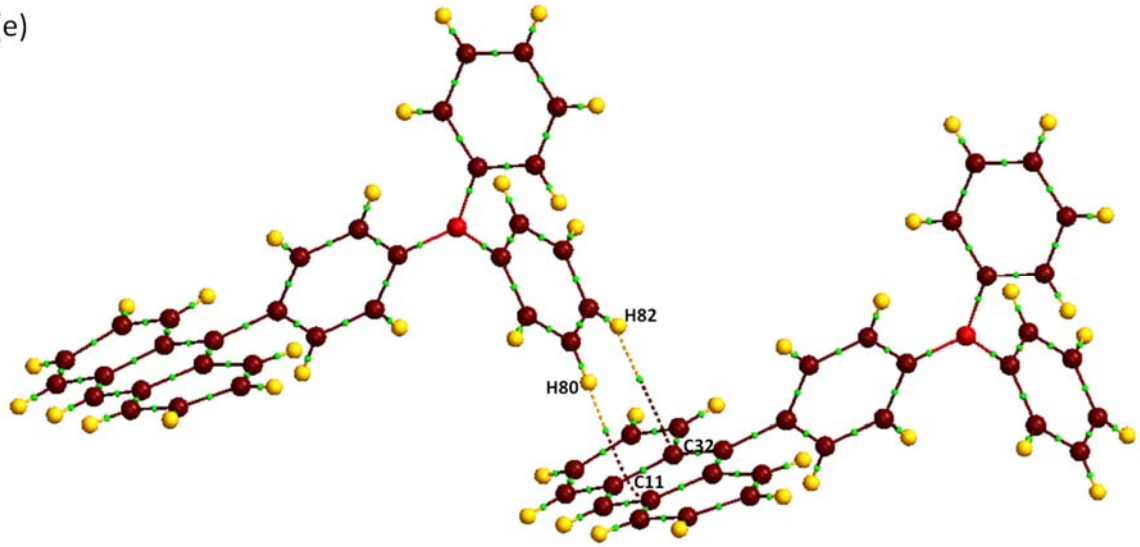

(f)

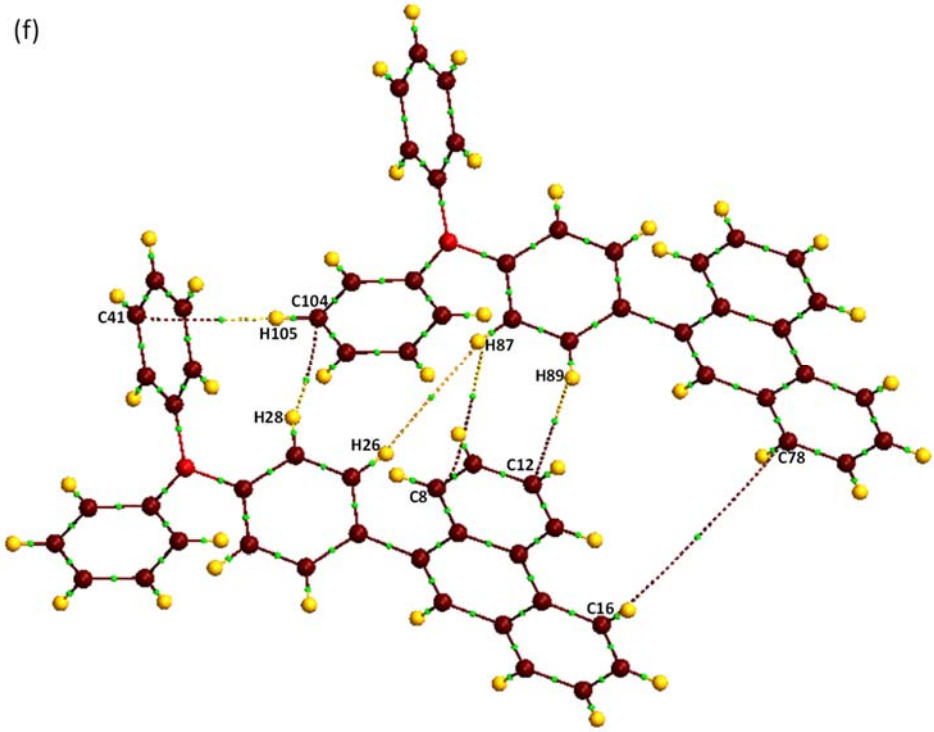

(g)

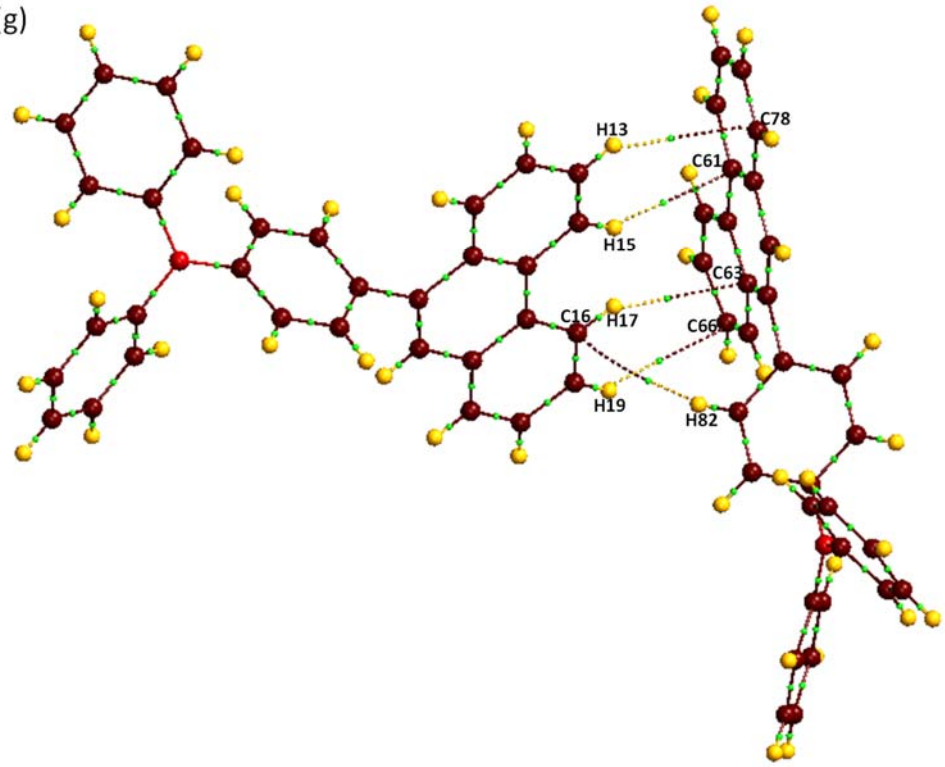
H13
C78
C61
H15
C63
C16
H17
C66
H19
H82

(h)

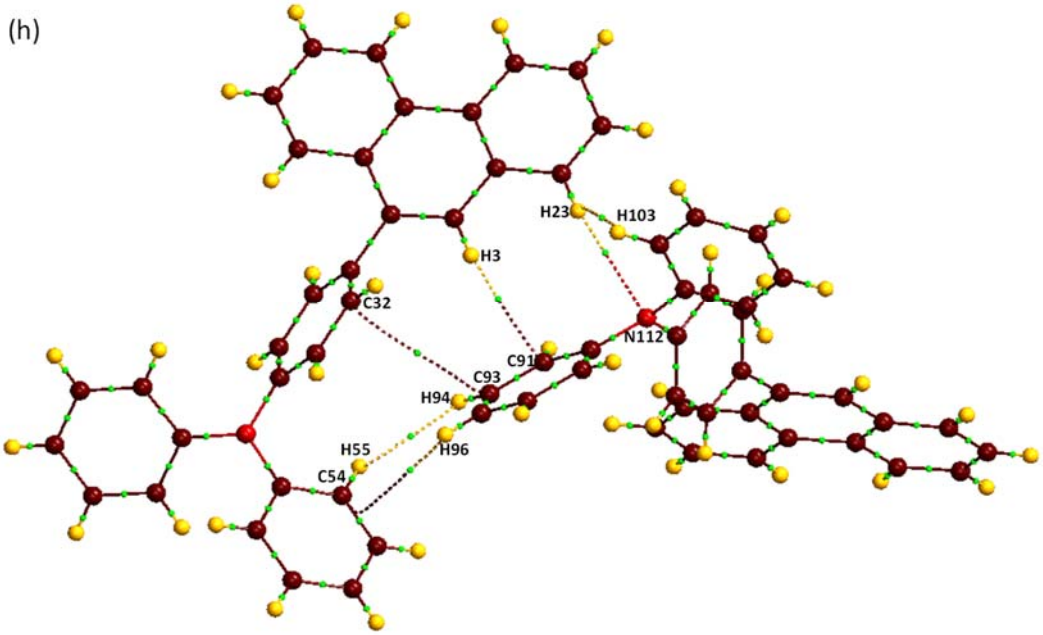
H23
H103
H3
C32
N112
C91
C93
H94
H55
H96
C54

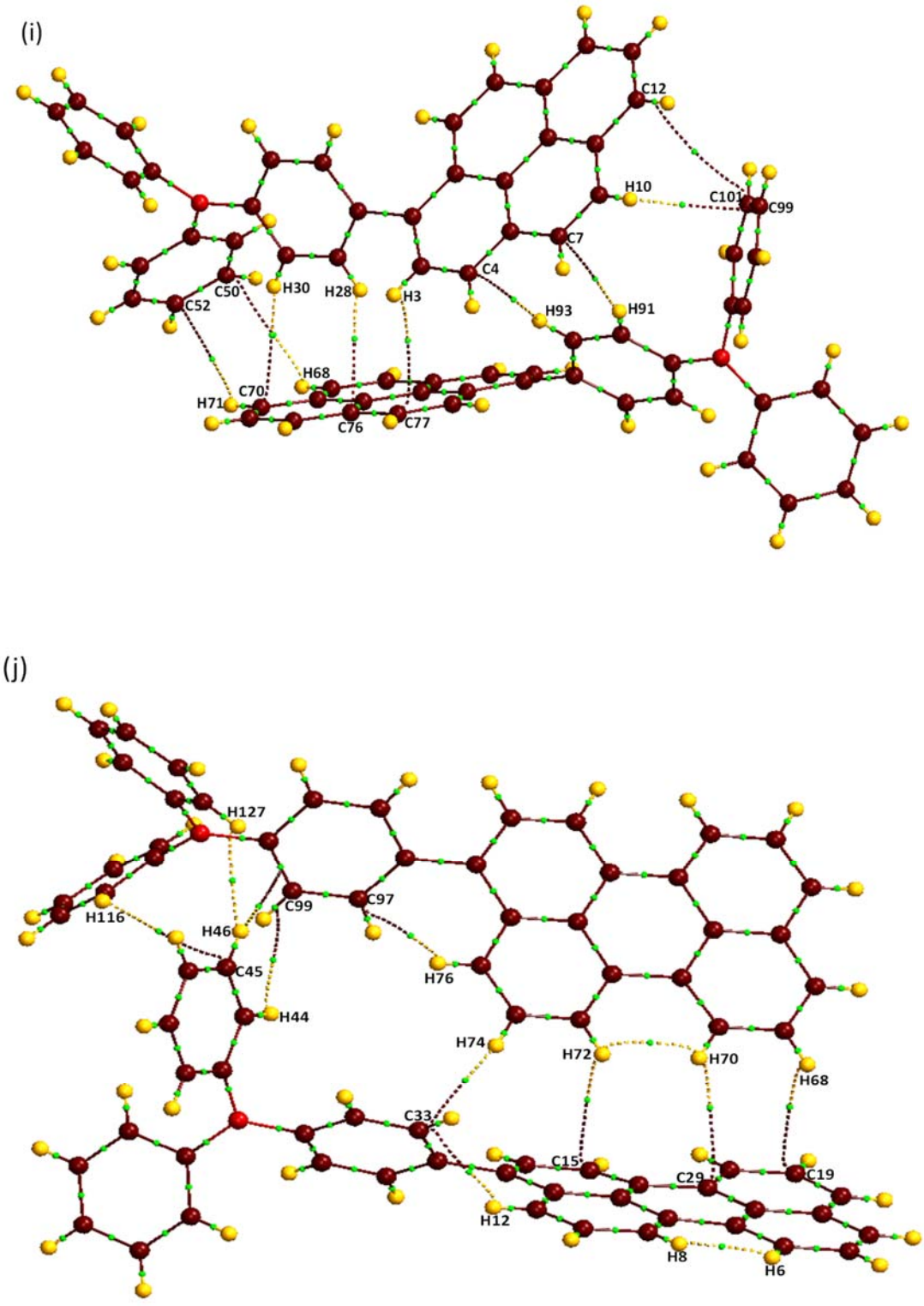

Fig. S5 QTAIM electron density maps of (a) PhTa, (b) PhTb, (c) NTa, (d) NTb, (e) AT, (f) PheTa, (g) PheTb, (h) PheTc, (i) PyT and (j) PeTb. Dotted lines shown are bond paths and the green dots are bond critical points (BCP). Bond path with a BCP indicate the existence of intermolecular interactions in different molecules.

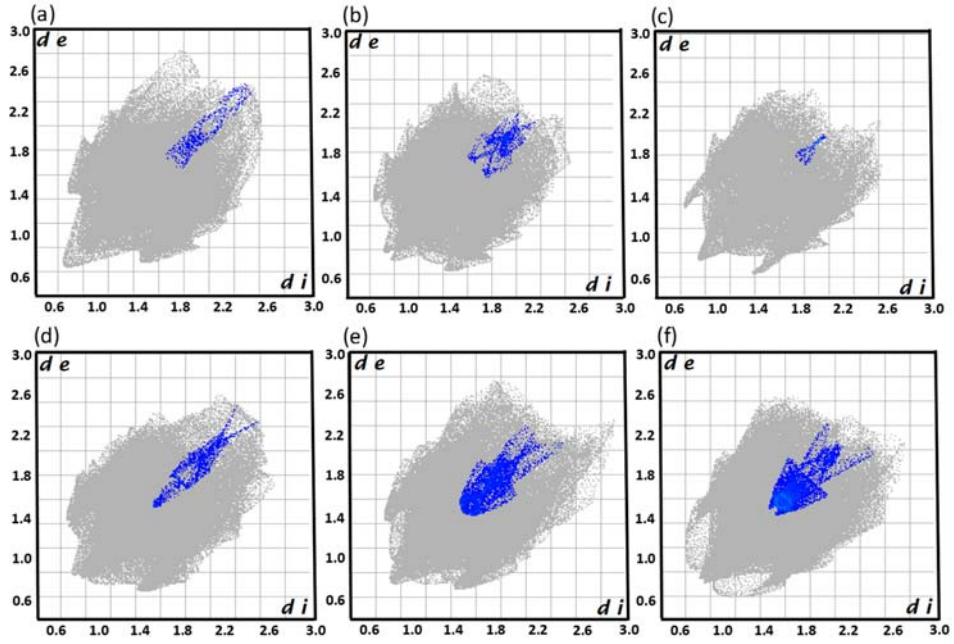

Fig. S6 2D-dimensional fingerprint plots representing C•••C interactions in crystalline (a) PhT, (b) NT, (c) AT, (d) PheT, (e) PyT and (f) PeT obtained from Hirshfeld analyses.

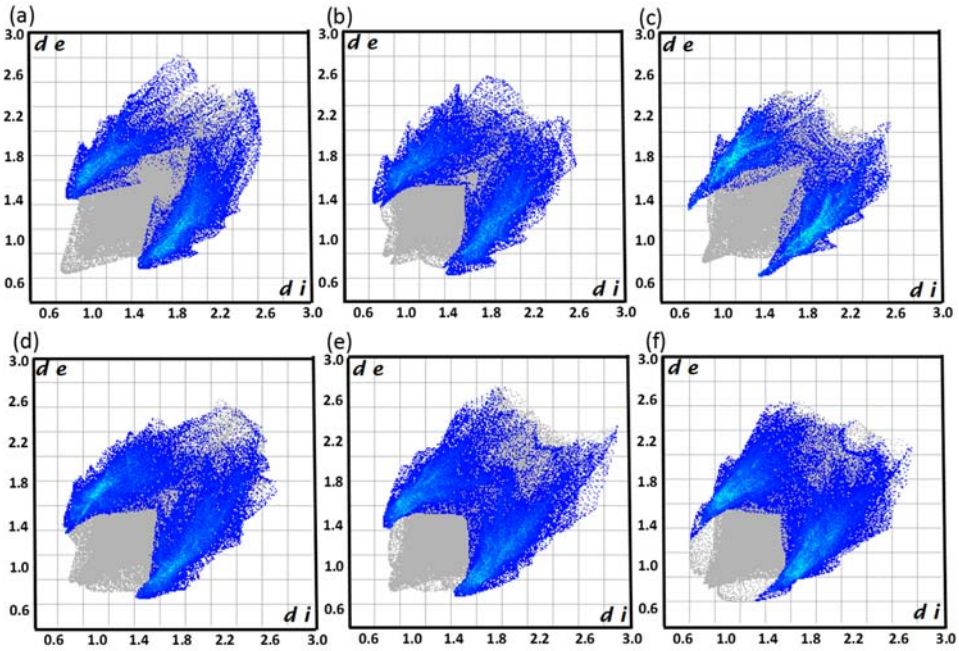

Fig. S7 2D-dimensional fingerprint plots representing C-H•••C interactions in crystalline (a) PhT, (b) NT, (c) AT, (d) PheT, (e) PyT and (f) PeT obtained from Hirshfeld analyses.

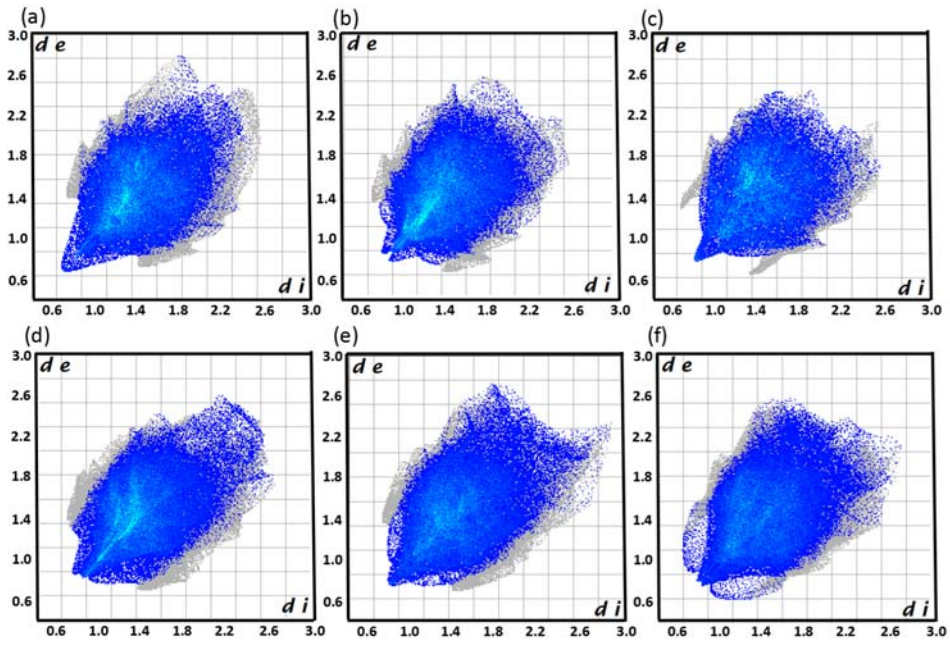

Fig. S8 2D-dimensional fingerprint plots representing C-H•••H-C interactions in crystalline (a) PhT, (b) NT, (c) AT, (d) PheT, (e) PyT and (f) PeT obtained from Hirshfeld analyses.

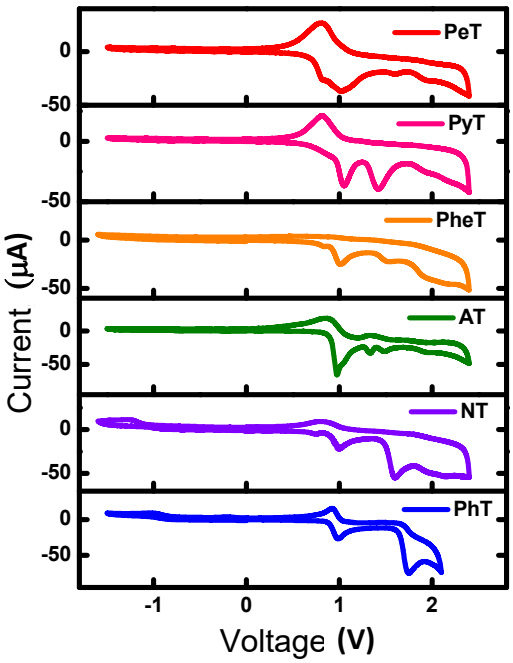

Fig. S9 Cyclic voltammetric measurements of ArT derivatives in DCM.

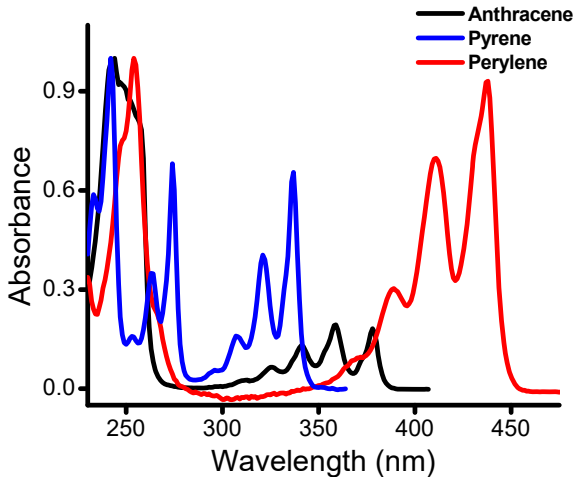

Fig. S10 The absorption spectra of anthracene, pyrene and perylene in DCM.

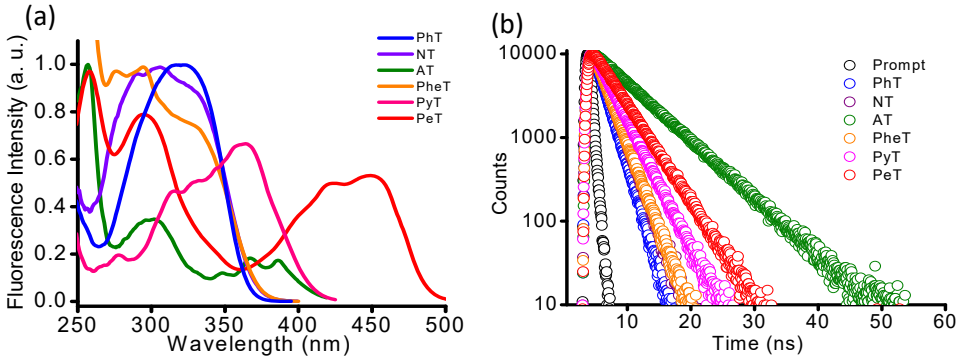

Fig. S11 (a) Excitation spectra and (b) fluorescent decay profile of ArT in DCM.

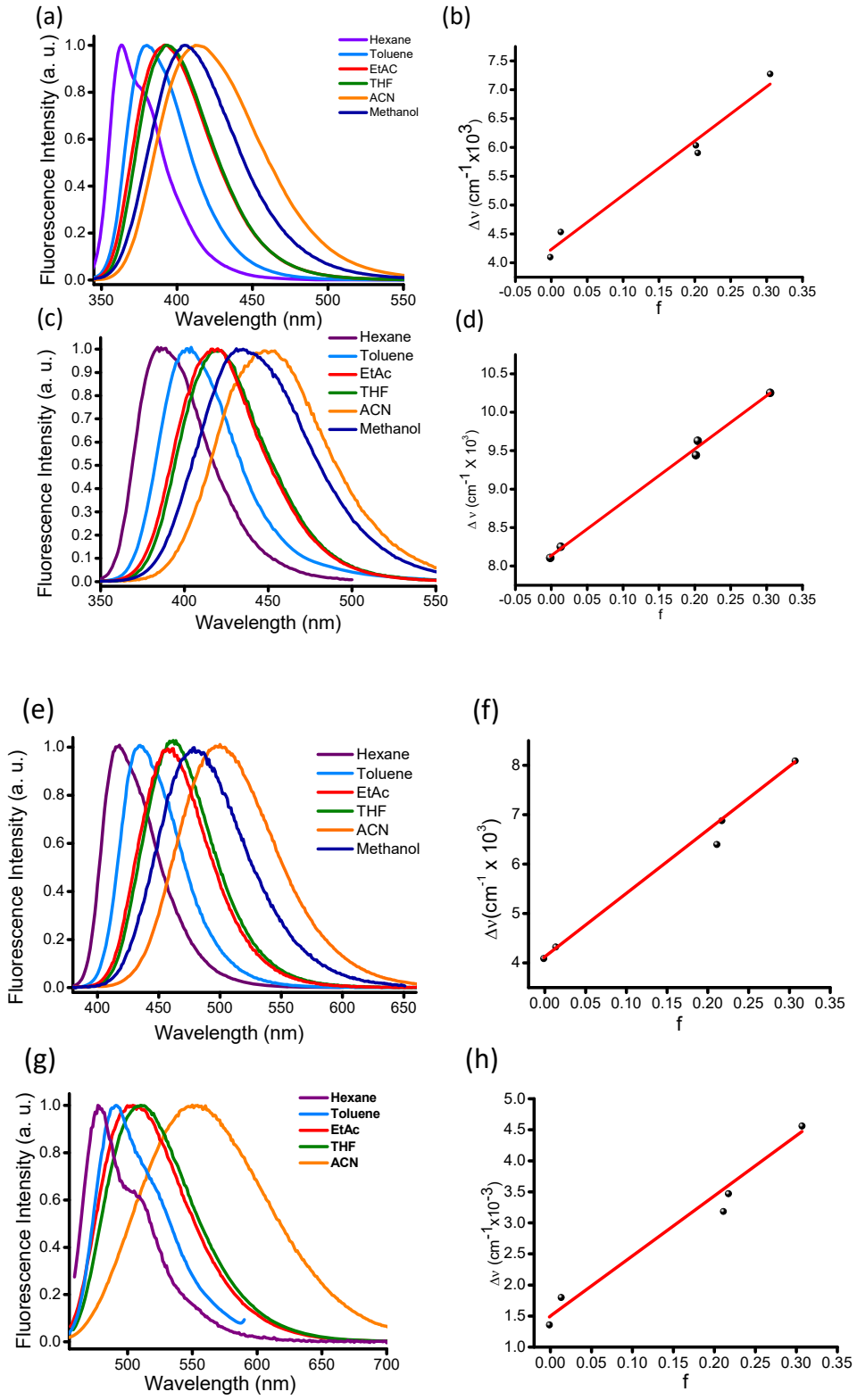

Fig. S12 Solvent polarity dependent normalized emission spectra of (a) PhT, (c) NT, (e) PyT and (g) PeT. Solvent polarity dependent Lippert-Mataga plots of (b) PhT, (d) NT, (f) PyT and (h) PeT.

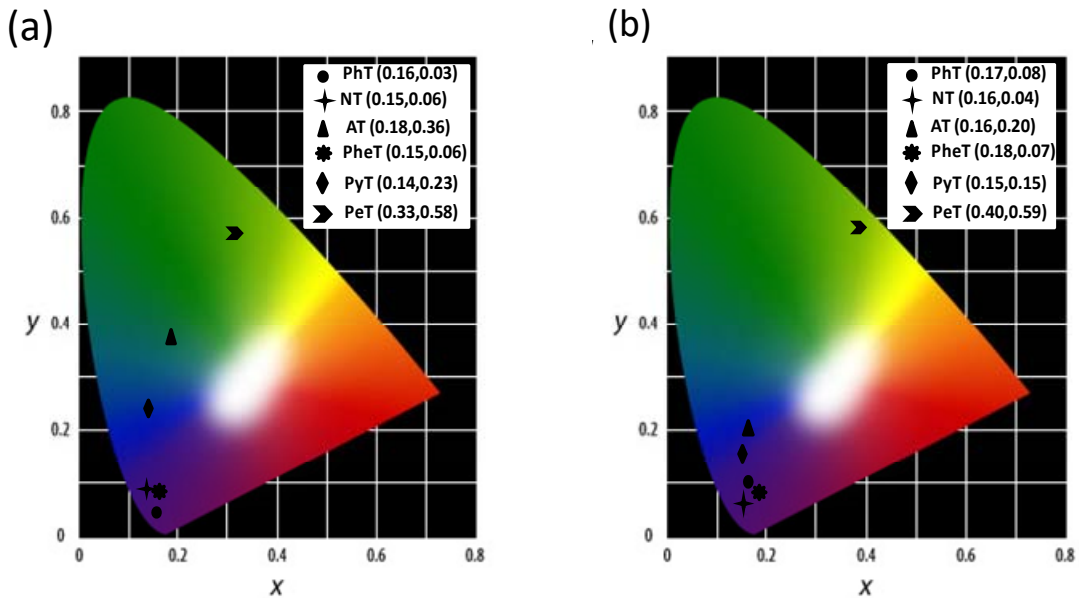

. **Fig. S13** CIE coordinates of ArT derivatives in (a) DCM and (b) crystalline state.

REFERENCES

1. J. R. Lakowicz, *Principles of Fluorescence Spectroscopy*, Springer, New York, 2006.
2. (a) E. Lippert and Z. Naturforsch, *Astrophys. Phys. Phys. Chem.*, 1955, 10, 541-545; (b) A. R. Mallia, P. S. Salini and M. Hariharan, *J. Am. Chem. Soc.*, 2015, 137, 15604-15607.
3. Gaussian 09, M. J. Frisch, G. W. Trucks, H. B. Schlegel, G. E. Scuseria, M. A. Robb, J. R. Cheeseman, G. Scalmani, V. Barone, B. Mennucci, G. A. Petersson, H. Nakatsuji, M. Caricato, X. Li, H. P. Hratchian, A. F. Izmaylov, J. Bloino, G. Zheng, J. L. Sonnenberg, M. Hada, M. Ehara, K. Toyota, R. Fukuda, J. Hasegawa, M. Ishida, T. Nakajima, Y. Honda, O. Kitao, H. Nakai, T. Vreven, J. A. Montgomery Jr., J. E. Peralta, F. Ogliaro, M. J. Bearpark, J. Heyd, E. N. Brothers, K. N. Kudin, V. N. Staroverov, R. Kobayashi, J. Normand, K. Raghavachari, A. P. Rendell, J. C. Burant, S. S. Iyengar, J. Tomasi, M. Cossi, N. Rega, N. J. Millam, M. Klene, J. E. Knox, J. B. Cross, V. Bakken, C. Adamo, J. Jaramillo, R. Gomperts, R. E. Stratmann, O. Yazyev, A. J. Austin, R. Cammi, C. Pomelli, J. W. Ochterski, R. L. Martin, K. Morokuma, V. G. Zakrzewski, G. A. Voth, P. Salvador, J. J. Dannenberg, S. Dapprich, A. D. Daniels, Ö. Farkas, J. B. Foresman, J. V. Ortiz, J. Cioslowski and D. J. Fox, Wallingford, CT, USA, 2009.
4. Z. E. X. Dance, S. M. Mickley, T. M. Wilson, A. B. Ricks, A. M. Scott, M. A. Ratner and M. R. Wasielewski, *J. Phys. Chem. A*, 2008, 112, 4194-4201.
5. A. R. Mallia, R. Sethy, V. Bhat and M. Hariharan, *J. Mat. Chem. C*, 2016, 4, 2931-2935.
6. P. Deng, L. Liu, S. Ren, H. Li and Q. Zhang, *Chem. Commun. (Cambridge, U. K.)*, 2012, 48, 6960-6962.
7. R. F. W. Bader, *Atoms in Molecules: A Quantum Theory*, Oxford University Press, Oxford, U.K., 1990.
8. (a) M. Yahia-Ouahmed, V. Tognetti and L. Joubert, *J. Chem. Theory Comput.*, 2015, 1053, 254-262; (b) M. A. Blanco, A. Martín Pendás and E. Francisco, *J. Chem. Theory Comput.*, 2005, 1, 1096-1109; (c) A. Martín Pendás, M. A. Blanco and E. Francisco, *J. Chem. Phys.*, 2006, 125, 184112.
9. H. Wang, W. Wang and W. J. Jin, *Chem. Rev.* , 2016, 116, 5072-5104.
10. *CrystalExplorer* 3.0, S. K. Wolff, D. J. Grinwood, J. J. McKinnon, M. J. Turner, D. Jayatilaka and M. A. Spackman, University of Western Australia, Perth, Australia, 2012.

11. R. Katoh, K. Suzuki, A. Furube, M. Kotani and K. Tokumaru, *J. Phys. Chem. C*, 2009, 113, 2961-2965.
12. I. B. Berlman, *Handbook of Fluorescence Spectra of Aromatic Molecules*, Academic Press, New York, 1971.